AIMS Energy, 13(5): 1347–1364.
DOI: 10.3934/energy.2025050
Received: 30 May 2025
Revised: 28 October 2025
Accepted: 06 November 2025
Published: 14 November 2025

https://www.aimspress.com/journal/energy

Research article

Numerical analysis of boiling in a horizontal pipe flow of a non azeotropic mixed mass

Chao Huang[1], Xiaohu Liu[1], Lijiao Gong[2,3], Mingting Wu[2,3,*] and Mingfei He[2,3,*]

[1] Xinjiang Tianfu Energy Co., Ltd., Xinjiang, Shihezi 832000
[2] School of Energy and Materials, Shihezi University, Shihezi, Xinjiang 832000, China
[3] Institute of Bingtuan Energy Development Research, Shihezi University, Shihezi, Xinjiang 832000, China

* **Correspondence:** Email: wumingting1995@163.com, mingfei_he@outlook.com.

Abstract: Non-azeotropic mixtures have attracted wide attention because they can reduce irreversible losses in heat exchangers and improve energy utilization efficiency. In this study, the heat and mass transfer characteristics during the boiling process of a non-azeotropic binary working-fluid mixture R601/R601a (1/3) in a horizontal tube (considering gravitational effects) were numerically analyzed using computational fluid dynamics (CFD) based on the VOF and k-ε turbulence models. The results indicate that the flow boiling behavior of the working fluid is strongly influenced by the coupling between thermal and hydrodynamic loads. Within the simulated operating range, when the inlet mass flow rate is low, the heat transfer coefficient becomes highly unstable, showing large fluctuations and poor overall heat transfer. With an appropriate increase in flow rate and heat-flux density, the heat-transfer performance improves significantly, and the Nusselt number becomes higher and more stable. At low flow rates, R601 reaches its saturation temperature, allowing vapor bubbles to pass through the main stream and form a vapor film near the upper wall. In contrast, the higher-boiling R601a undergoes only subcooled boiling, where bubbles shrink or collapse within the subcooled liquid core and cannot reach the upper wall. The observed two-phase flow differences are dominated by the boiling points of the components and the degree of subcooling in the main flow.

Keywords: non azeotropic; binary mixed media; horizontal tube; flow boiling; numerical analysis

1. Introduction

With the development of low-temperature waste heat utilization research, the organic Rankine cycle has been widely applied and studied for its simple system structure and lower evaporating pressure and temperature [1,2]. In the intensive heat transfer studies of evaporators and condensers, non-azeotropic coolants utilize solution components with boiling points ranging from low to high to undergo boiling sequentially, and the working fluid can be continuously maintained in the nucleate boiling state, thus enabling the thermal efficiency of the pipeline to be improved [3]. This type of coolant holds great promise for the development of coolant types, range of use, and improvement of system performance, as well as the realization of graded energy utilization. Non-azeotropic hybrid coolants have temperature slip characteristics when the gas-liquid two-phase changes, and can be matched with variable-temperature heat sources in practical engineering to effectively reduce the available energy loss of the system and improve the system efficiency [4–6]. Compared with the pure fluid, a non-azeotropic mixed fluid can effectively delay or even avoid the occurrence of the dry-out phenomenon, even at lower mass flow rates of higher heat flux density of the working conditions are not prone to significant deterioration of heat transfer, greatly improving the reliability of the heat exchanger [7–9]. This is a typical flow-boiling process.

Existing studies have mainly explored the flow and boiling heat transfer characteristics of non-azeotropic mixtures by means of experiments and numerical simulations. For numerical simulation, Banerjee R [10] used numerical simulation to investigate the evaporation rate of gas-liquid phase of a mixture of ethanol and iso-octane in countercurrent flow in an inclined two-dimensional channel, and the results showed that the interfacial heat transfer and mass transfer of the mixture was significantly higher than that of its pure component. In the countercurrent flow system, the interfacial heat and mass transfer coefficient is higher near the channel outlet, and decreases from the channel outlet to the channel inlet. Barroso-Maldonado JM et al. [11] predicted and analyzed the frictional pressure drop of a non-azeotropic mixed-working fluid boiling in a flow at low temperatures based on an artificial neural network. He et al. [12] established a numerical simulation model for the evaporative heat transfer of hydrocarbon coolant CH4/C2H6 in a multi-spiral winding tube. The flow transition and heat transfer characteristics of mixed media with different component ratios were obtained through numerical simulation, and the flow diagrams were plotted. Zhang et al. [13] numerically analyzed the condensation heat and mass transfer process of a non-azeotropic binary vapor mixture on a vertical wall under the condition of natural convection, used cyclohexane and water as the non-azeotropic media, and analyzed the effects of vapor mass concentration and wall subcooling on the condensation pattern and heat and mass transfer of the mixed vapors. The effects of vapor mass concentration and wall subcooling on the condensation pattern and heat and mass transfer were analyzed. Wang et al. [14] numerically simulated the falling film evaporation of a non-azeotropic refrigerant consisting of R32 and R134a outside of a horizontal tube, and investigated the effects of operating parameters, such as the spray height, tube diameter, inlet temperature, Reynolds number, heat flux density, and the mass fraction of the working fluid, on heat transfer coefficients. Lv et al. [15] numerically simulated the heat transfer coefficients of a binary heat transfer characteristics of a working-fluid mixture in a horizontal microtube, and obtained the influence law of steam mass, heat flow density, mass flow rate, ethane mole fraction, and other factors on the boiling heat transfer characteristics.

On the experimental side, Xu et al. [16] analyzed the bubble dynamics evolution process and the correlation mechanism between flow pattern and heat transfer for the flow and heat transfer

characteristics of a non-azeotropic mixture of working fluids in a special rhombic finned microchannel of a printed circuit heat exchanger at an angle of 22.6°. The results show that the rhombic microrib channel is more stable than the straight microchannel flow, and a new correlation equation is established to predict the subcooled boiling HTC of non-azeotropic mixtures in the rhombic microrib channel. Chen et al. [17] experimentally investigated the non-azeotropic mixtures of different mass fractions (80/20, 70/30, and 60/40) of R1233zd(E)/R1234yf, in an 8-mm-ID tube. Lu et al. [18] experimentally investigated the flow-boiling heat transfer characteristics of mixed fluids R1233zd(E)/R1234yf with different fractions, and proposed a new heat transfer coefficient prediction equation. Dai et al. [19] experimentally investigated the flow-boiling characteristics of the mixed fluids CO_2/R152a with different fractions in a 2-mm horizontal tube and compared with that of the pure fluid. In their comparison, the heat transfer and pressure drop characteristics of the working fluid were analyzed, the flow pattern was plotted, and a new relationship equation for the heat transfer coefficient was proposed. The results showed that seven different flow patterns appeared in the microchannels of mixed working fluids. Huang et al. [20] used an experimental method to simulate the high-temperature boiling of non-azeotropic mixtures R134a/R245fa in plate heat exchangers, and evaluated several existing methods for predicting heat transfer coefficients and pressure drop, based on which new prediction equations were developed. Qi et al. [21] studied the heat transfer coefficient and pressure drop characteristics of four azeotropic mixtures R134a/R245fa with different compositions (20/80, 37/63, 52/48, and 60/40), and compared them with the flow-boiling compositional changes and heat transfer characteristics of pure R245fa in a rectangular channel to reveal the effects of the liquid composition and thermal invariants. Wang et al. [22] focused on the study of the horizontal smooth tubes and microfinned tubes with different mass fractions of R245fa/R141b, and boiling heat-transfer coefficients and pressure-drop variations were obtained experimentally.

In summary, the CFD numerical simulation method offers significant advantages in the study of boiling heat transfer for non-azeotropic mixtures. It is capable of capturing transient interfacial behaviors (such as bubble nucleation and component concentration gradient distribution) that cannot be directly observed in experiments. While experimental studies provide benchmark data for the flow boiling of non-azeotropic mixtures, their measurement methods are limited in resolving microscopic phase interface behaviors. Therefore, the advantage of this paper lies in the use of a CFD-based numerical approach to simulate and analyze the heat transfer mechanisms of the R601/R601a mixture in a horizontal tube. By fully leveraging the power of CFD, this study provides a comprehensive understanding of the flow boiling characteristics of the R601/R601a binary non-azeotropic refrigerant, and offers valuable theoretical insights for its application as a cooling fluid. This study simulates the complex two-phase flow dynamics and heat transfer phenomena of the R601/R601a binary non-ideal volatile mixture, which previous studies have not fully covered, significantly enriching the theoretical framework for the use of such binary mixtures in cooling applications.

2. Numerical calculation

2.1. Physical model

The geometric model of a square-section horizontal pipe is shown in Figure 1. The working fluid flows in from the left end of the pipe and out from the right side after being heated by a single side wall at the bottom of the pipe, with a section of adiabatic wall at the inlet and outlet to eliminate end

effects. The inlet temperature of the working fluid is 299 K. The inlet volume fraction ratio of R601 and R601a mixed working fluid is 1:3. The calculation method of the physical property parameters in this paper is based on the hydrocarbon-thermal-property calculation program REFPROP developed by NIST. To apply these thermal properties in the numerical calculations, we adopted a piecewise linear interpolation method to fit the thermal property data at different temperatures and pressures into piecewise-linear functions, which were then imported into Fluent for numerical simulation. The physical property parameters of the components under the operating conditions are shown in Table 1, and the numerical calculation conditions are shown in Table 2. The selected parameter conditions are based on common flow boiling conditions and typical working ranges in practical engineering applications, with reference to the operating conditions and parameter ranges in [21]. q denotes the heat flux density, and v represents the inlet velocity.

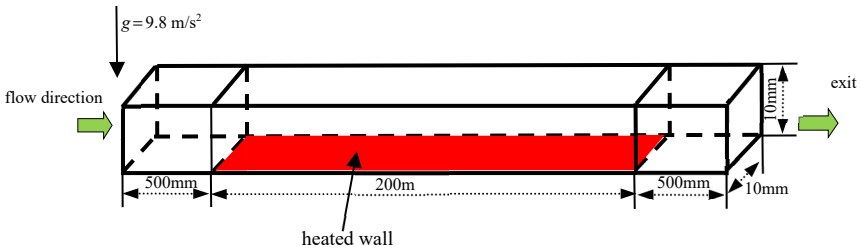

Figure 1. Geometric model.

Table 1. Physical properties of components.

	Liquid phase R601	Gas phase R601	Liquid phase R601a	Gas phase R601a
Density ρ(kg/m^3)	610.365	2.938	612.4699	3.0187
Constant pressure specific Heat C_p(J/kg·K)	2366.5	1755.6	2286.8	1711
Thermal conductivity k(W/m·K)	0.108	0.0156	0.101	0.0146
Dynamic viscosity μ(kg/m·s)	2.0022×10^{-4}	6.96879×10^{-6}	2.14318×10^{-4}	7.06946×10^{-6}
Standard boiling point$T$(K)	301		309	

Table 2. Numerical calculation working conditions.

q / v	10 kW/m^2	25 kW/m^2	50 kW/m^2	100 kW/m^2
0.1 m/s	case 1	case 2	case 3	case 4
0.3 m/s	case 5	case 6	case 7	case 8
0.5 m/s	case 9	case 10	case 11	case 12

2.2. Physical model

Based on the computational fluid dynamics software ANSYS Fluent [23], a fluid volume model [24] is used as a multiphase flow model to capture the vapor-liquid phase interface information, and the control equations used are:

$$div(\rho\vec{V}\Phi) = div(\Gamma\Delta\Phi) + S \tag{1}$$

where ρ is the density, kg/m^3; v is the velocity vector, m/s; Φ is the band seeking scalar, J/kg; Γ is the generalized diffusion coefficient of Φ, kg/(m·s); $\Delta\Phi$ is the gradient of Φ; and S is the generalized source term per unit volume of Φ, W/m^3.

Surface tension was modeled using the continuum surface force (CSF) model developed by Brackbill [25], ultimately treated as a function of the pressure jump at the phase interface.

$$\vec{F}_{vol} = \sigma \frac{\alpha_L \rho_L \kappa_L \nabla \alpha_L + \alpha_V \rho_V \kappa_V \nabla \alpha_V}{(1/2)(\rho_L + \rho_V)} \tag{2}$$

where σ is the surface tension coefficient, N/m; and κ is the curvature of the phase interface, respectively.

$$\kappa_V = -\kappa_L = -\nabla \cdot \left(\frac{\nabla \alpha_V}{|\nabla \alpha_V|} \right) \tag{3}$$

The mass transfer from evaporation and boiling is solved by adding the corresponding mass source terms, and the VOF model treats E in the energy equation as the volume fraction total energy.

$$E = \frac{\alpha_L \rho_L E_L + \alpha_V \rho_V E_V}{\alpha_L \rho_L + \alpha_V \rho_V} \tag{4}$$

where $E_L = C_{p,L}(T - 298.15)$, $E_V = C_{p,V}(T - 298.15)$, J/kg. The widely used Lee [26] phase transition model is chosen to deal with the boiling and condensation processes, and the energy transfer term $Q = h_{LV}S_L$ is solved by S_L and S_V.

$$S_L = r_L \alpha_L \rho_L (T_L - T_{SAT})/T_{SAT} \quad T_L \geq T_{SAT} \tag{5}$$

$$S_V = r_V \alpha_V \rho_V (T_{SAT} - T_L)/T_{SAT} \quad T_V < T_{SAT} \tag{6}$$

where r is an empirical constant reflecting the mass transfer intensity factor, s^{-1}. Considering all factors, the value of r is set to 5, where r is the empirical constant reflecting the mass transfer intensity factor, set to 5. α_L and α_V represent the volume fractions of the liquid and vapor phases, respectively, while ρ_L and ρ_V are the densities of the liquid and vapor phases, respectively. T_{SAT} denotes the saturation temperature, and T is the temperature of the fluid.

The heat transfer coefficient is defined as follows:

$$h=\frac{q}{T_w+T_b} \tag{7}$$

where q is the wall heat flux, T_w is the wall temperature, and T_b is the bulk fluid temperature.

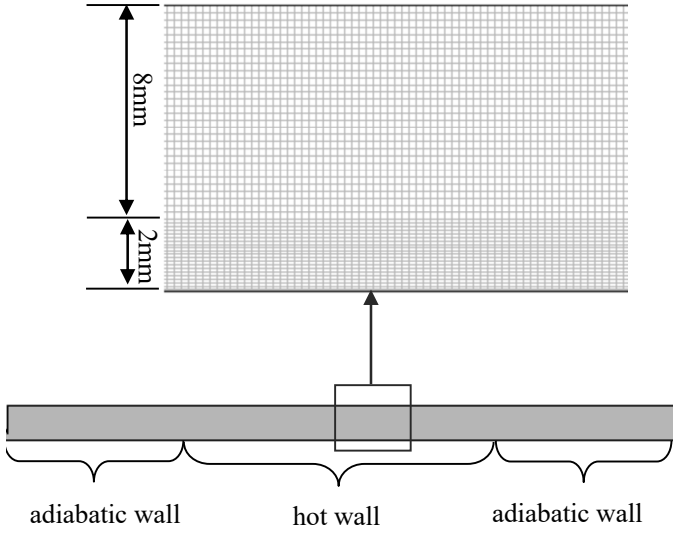

Figure 2. Meshing of the physical model.

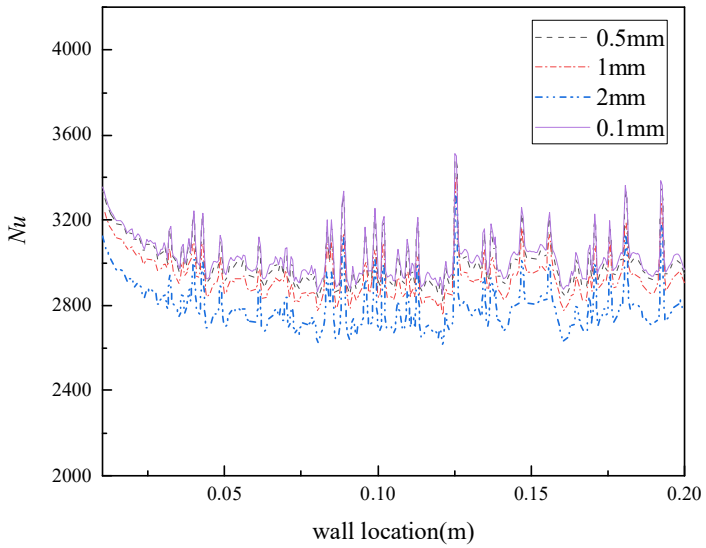

Figure 3. Comparison of numerical calculation results for different grid sizes.

The physical model was meshed using the Gambit software, as shown in Figure 2. The results for four distinct grid resolutions are presented in Figure 3. The analysis reveals that as the grid size increases from 0.5 to 1.0 mm, the deviation in the Nusselt number values becomes significantly larger compared to the baseline case with the 0.1 mm grid. Balancing computational cost and accuracy, a grid size of 0.5 mm was selected for subsequent simulations. In order to accurately obtain the growth and

movement of the wall vapor bubbles, the grid was encrypted at the boundary layer. A fixed time step of 1×10^{-5} s was used for unsteady-state calculation.

The inlet boundary condition is a velocity inlet, the outlet is a pressure outlet, a constant heat flux density is applied to the heated wall, and the rest is an adiabatic wall. The convective term of the control equation is discretized using the second-order upwind scheme, and the PRESTO! pressure interpolation scheme is used as the differential format of the pressure equation. The pressure–velocity coupling was solved using the PISO (Pressure Implicit with Splitting of Operators) algorithm. All residuals less than 10^{-5} were used as the convergence criterion.

3. Discussion

3.1. Validation of numerical methods

In order to verify the accuracy of the numerical model, the distribution of heat transfer enhancement values Nu/Nu_0 obtained from numerical calculations was compared with the experimental test results of Ekkad et al. [27] using the same model under the same operating conditions, as shown in Figure 4, where Nu is the local Nusselt number.

$$Nu = \frac{h \cdot d}{k} \tag{8}$$

where h is the convective heat transfer coefficient of the fluid, W/(m^2·K); and k is the thermal conductivity of the fluid, W/(m·K); and Nu_0 is the empirical Nu number corrected by Dittus-Boelter/McAdams.

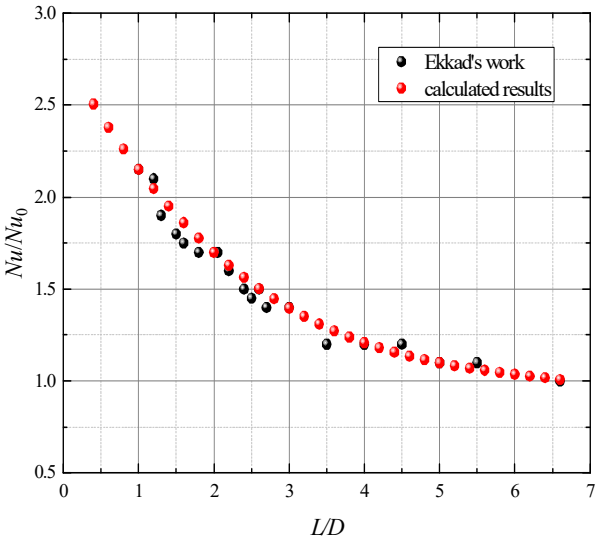

Figure 4. Comparison of numerical calculations with experimental measurements by Ekkad et al. [27].

$$Nu_0 = 0.023\,\mathrm{Re}^{0.8}\,\mathrm{Pr}^{0.4} \tag{9}$$

where Pr is the Prandtl number.

Comparison with the experimental results of Ekkad et al. [27] shows that the deviation between the numerical results and the experimental data was less than 5%, which is in good agreement. The temperature distribution obtained from numerical calculations is compared with the experimental data from Chiou et al. [28], as shown in Figure 5, and the consistency is good.

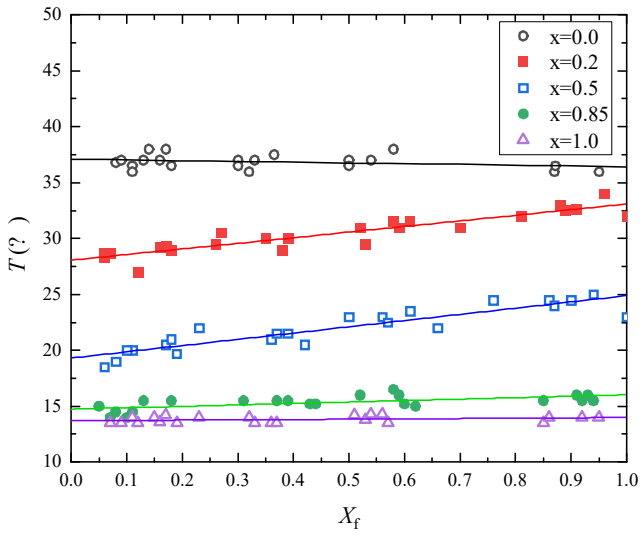

Figure 5. Comparisons between numerical simulation and Chiou's [28] experimental measurements.

3.2. Effect of heat flow density on heat transfer characteristics

A sub-component display of the volume fraction distribution cloud of two kinds of working gases in the pipe at an inlet flow rate of 0.1 m/s is shown in Figure 6, where (a) shows the volume distribution cloud of R601 gas phase in R601 liquid, and (b) shows the volume distribution cloud of R601a gas phase in R601a liquid. It is easy to see that with the increase of the wall heat flux density, the boiling degree of the fluid in the pipeline gradually increases and is in different stages of the nucleate boiling state. Under the high heat flux density condition, the gas is dramatically concentrated at the upper wall surface of the pipe, forming a gas film. Comparison of the cloud diagrams of the volume fraction distribution of sub-component gas phases shows that R601, which has a lower boiling point, reaches boiling earlier than R601a, and the degree of boiling is more intense. Comparison of the density distribution plots of the mixed working fluids shows that the gas–liquid distribution characteristics of the mixed working fluids are mainly controlled by the low-boiling-point R601, despite the higher proportion of R601a in the mixture.

The Nusselt number and temperature distribution curves of the hot wall surface under different wall heat flux density conditions are shown in Figure 7. With the increase of wall heat flux density, the Nu number on the wall surface increases significantly; however, the relationship between Nusselt number and wall heat flux density gradually slows down, which is in line with the general law of convective heat transfer. At a given working condition, the occurrence of nucleate boiling causes the distribution of Nusselt number on the hot wall surface to have an oscillatory characteristic distribution. That is, at the core point of gasification, the wall cavities absorb heat by phase change, and the Nusselt number increases; after the formation of bubbles, the wall heat transfer conditions deteriorate at the bubble coverage, and Nu decreases. Bubbles are formed at different locations on the hot wall surface,

which results in an oscillating distribution of the wall Nusselt number. At q = 100 kW/m², the dense bubbles formed on the hot wall surface cause a larger fluctuation amplitude due to their merger and aggregation, affecting the wall Nusselt number, and the fluctuation amplitude of Nu is comparable at q = 10 kW/m² and q = 25 kW/m².

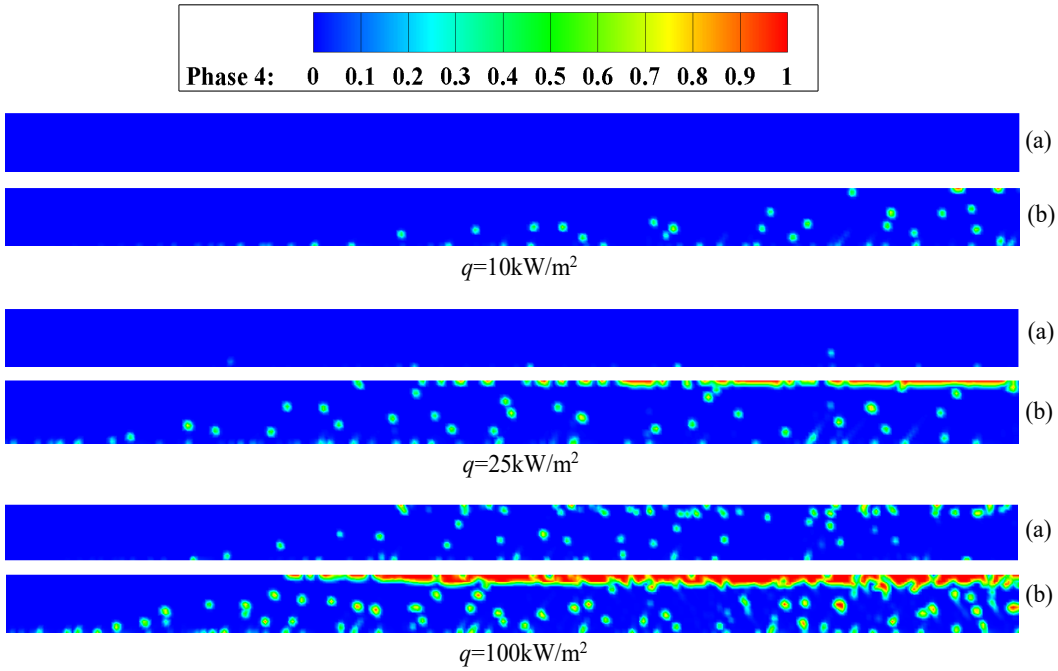

Figure 6. Cloud view of fluid gas phase volume fraction distribution in the tube at 2 s. (a) R601 (b) R601a.

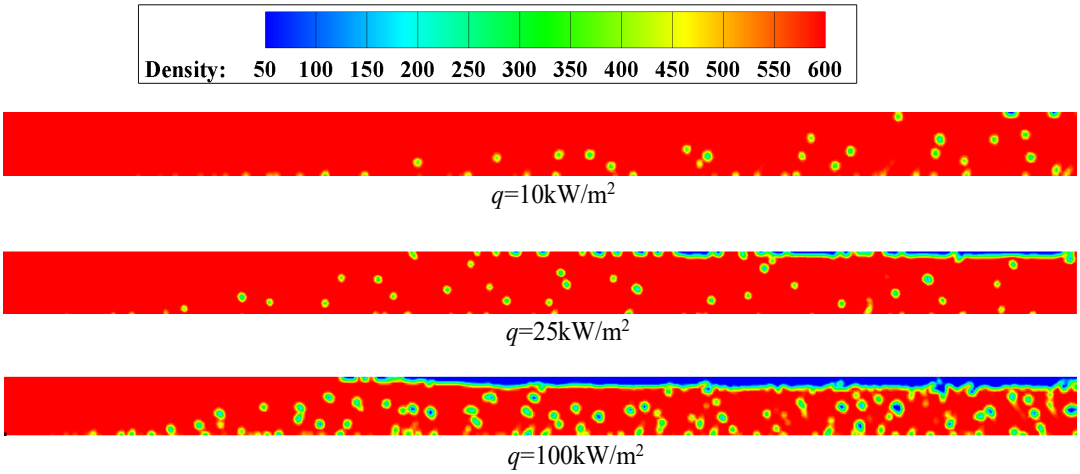

Figure 7. Cloud view of fluid density distribution in the tube at 2 s.

In contrast, the wall temperature distribution pattern is more obvious at different heat flux densities, as illustrated in Figure 8. The higher the heat flux density, the higher the wall temperature

base, the higher the fluctuation amplitude, and the higher the fluctuation frequency. The phenomenon can be explained by the bubble distribution on the hot wall surface. At low wall heat flux density, the hot wall surface bubble distribution is sparse, the mainstream is still in subcooled boiling, and the hot wall surface temperature fluctuates weakly near the base value. At high wall heat flux density, the hot wall surface bubble distribution is dense, the mainstream has long reached saturation boiling, and the hot wall surface temperature fluctuates around the base value with a high-frequency oscillation.

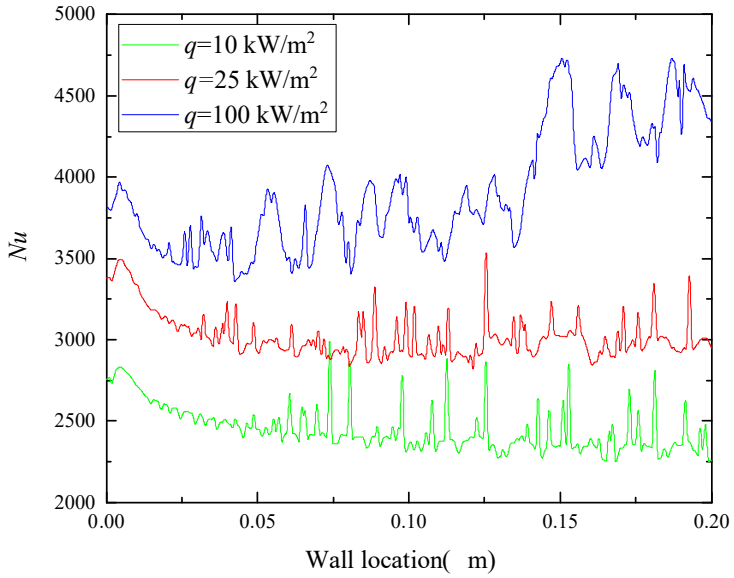

(a) Nusselt number

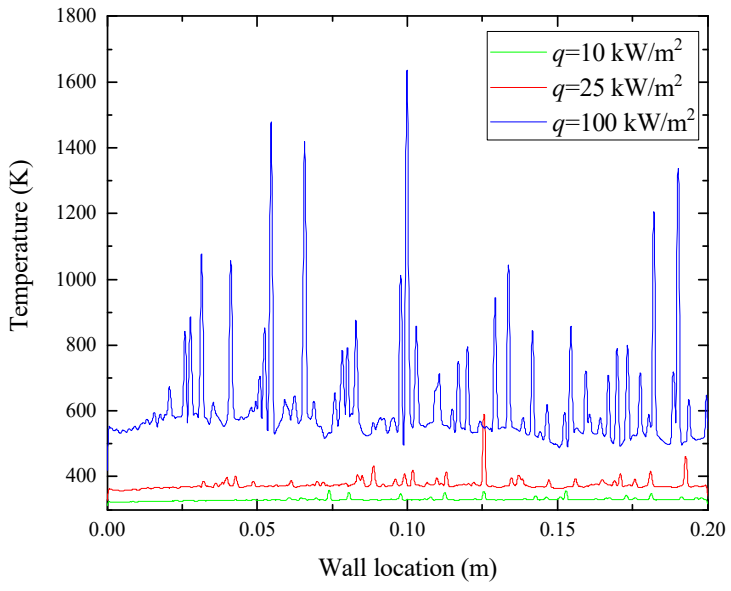

(b) Temperature

Figure 8. Parameter distribution profile on the hot wall surface at 2 s for different heat flow densities.

In addition, the results highlight the dominant role of the more volatile R601 component in determining the flow boiling behavior. Due to its lower boiling point, R601 reaches boiling earlier,

which significantly influences the vapor distribution and heat transfer characteristics in the system. As the flow velocity increases, the higher volatility of R601 leads to enhanced bubble formation, which further accelerates the boiling process and improves heat transfer efficiency. This behavior underscores the importance of considering the volatility differences between components when designing non-azeotropic mixture heat exchangers. The dominant role of R601 in the boiling process means that a higher proportion of this component can potentially lead to a more efficient heat transfer mechanism, especially in systems that rely on phase-change heat transfer. In contrast, the higher boiling R601a component acts to stabilize the process, reducing fluctuations in temperature and improving system stability. Therefore, understanding the interplay between these components and adjusting operational conditions accordingly can significantly enhance the design and performance of non-azeotropic mixture-based heat exchangers.

3.3. Effect of inlet flow rate on heat transfer characteristics

The cloud diagram of the distribution of the gas-phase volume fraction of each component at different flow rates is shown in Figure 9 for q = 25 kW/m². From the figure, it can be seen that with the increase of flow rate, the degree of fluid boiling in the pipeline is gradually weakened. Under the low flow rate condition, the R601 component is able to reach the saturation temperature, and the bubbles are able to pass through the main flow after being generated from the surface of the hot wall, and gather above the pipe wall to form a thin gas film. The high-boiling-point R601a component can only undergo subcooled boiling; the bubble formed on the surface of the hot wall in the subcooled mainstream contracts or even collapses and cannot reach the upper wall surface of the pipeline. At v = 0.3 m/s, the R601 component is also in the subcooled boiling state, and the mainstream temperature is difficult to reach the saturation state. At v = 0.3 m/s, when the boiling point of the R601a component is high, as well as at v = 0.5 m/s, both components are in the convective heat transfer state, and the superheat of the fluid on the surface of the hot wall is not enough for the occurrence of nucleate boiling.

It is evident that, in the non-azeotropic mixture studied in this work, the low-boiling, volatile R601 component dominates the early stages of vaporization, driving the phase change and flow behavior. The bubble formation and coalescence processes of R601 determine the local vapor phase distribution and the structure of the heat transfer pathways. As the flow velocity increases, the dominance of R601 gradually diminishes, and the system transitions from a boiling-dominated to a convection-dominated heat transfer regime.

The cloud plots of the overall density distribution of the fluid in the tube at different flow rates are shown in Figure 10, and the cloud plots of the distribution of the gas-phase volume fractions of the core components show that the gas–liquid distribution characteristics of the mixed working fluids are mainly controlled by the low-boiling-point R601, even though R601a occupies a higher proportion in the mixtures.

The graphs of Nusselt number and temperature distribution on the hot wall surface as well as the average *Nu* and average temperature distribution at different flow rates are shown in Figure 11. With the increase of the flow rate in the tube, the *Nu* of the wall surface increases significantly, which is in line with the general law of convective heat transfer. The interesting phenomenon is that the distribution of *Nu* is first a smooth curve when the tube is in the convective heat transfer stage; then, the *Nu* begins to oscillate with a certain frequency and gradually increasing amplitude when the tube is in the subcooled heat transfer stage, and the gradual formation of air pockets on the hot wall surface

causes the oscillation of *Nu*. The amplitude of this oscillation gradually decreases with the increase of flow rate, which means that in this paper, the faster the flow rate, the more stable the heat transfer effect of the tube wall, the regularity of the *Nu* oscillation is then disrupted, and nucleate boiling occurs in the tube. It is not difficult to see that the location where the *Nu* regularity is disturbed is gradually shifted forward, indicating that the location where the nucleate boiling state appears is gradually shifted forward, which is consistent with the display of the previous phase-distribution cloud diagram. In addition, the amplitude values of the *Nu* oscillations are of comparable magnitude at different flow rates, reflecting the comparable sizes of the bubbles generated on the hot wall surface at these flow rates.

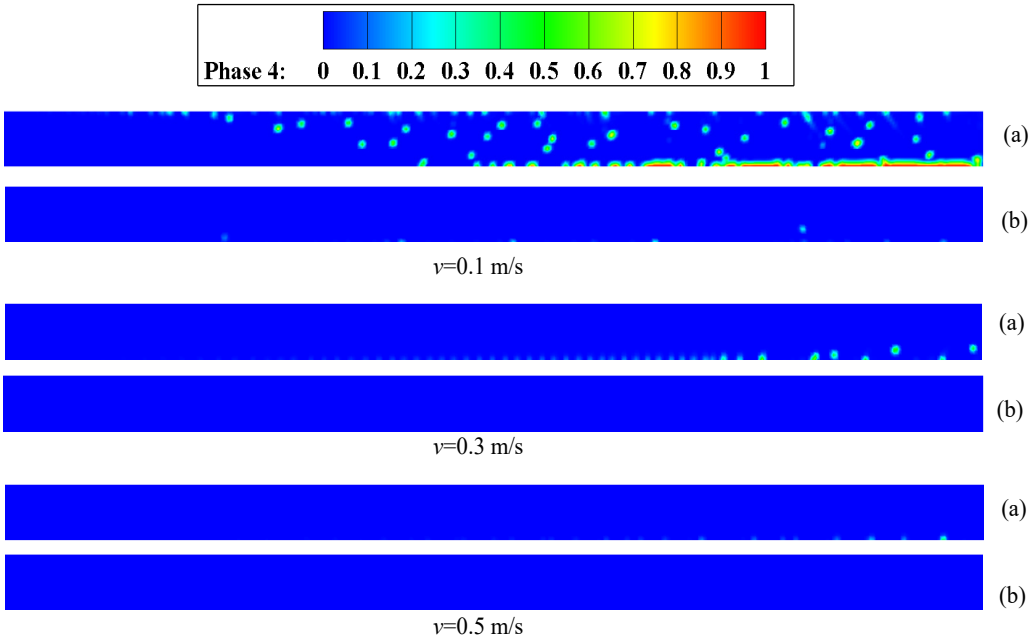

Figure 9. Cloud view of fluid vapor phase distribution in the tube at 2 s. (a) R601 (b) R601a.

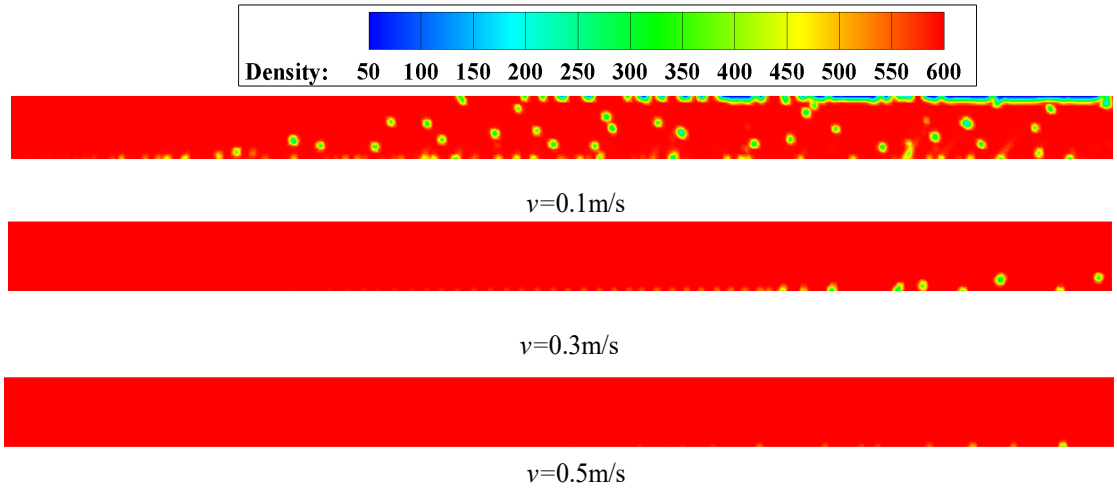

Figure 10. Cloud view of fluid density distribution in the tube at 2 s.

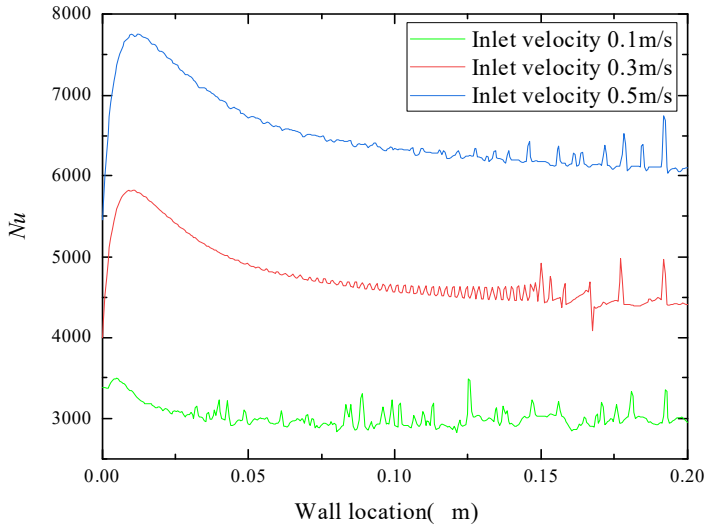

(a) Nusselt number

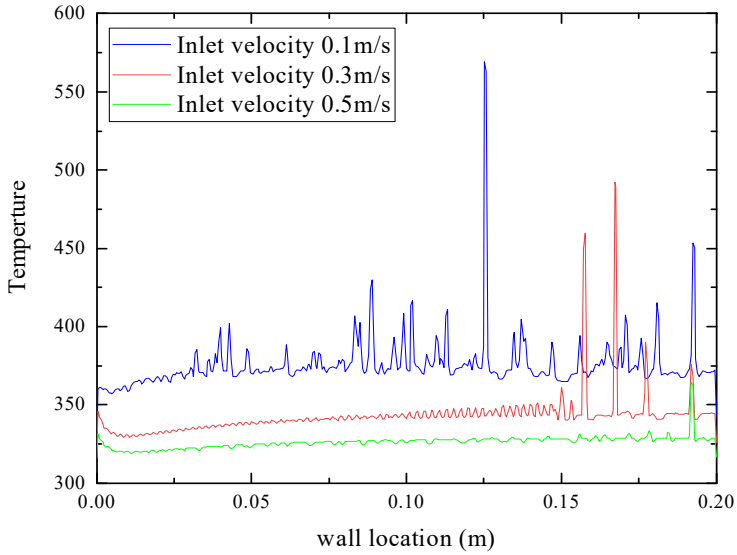

(b) Temperature

Figure 11. Parameter distribution profiles on the hot wall surface at 2 s for different flow rates.

The distribution pattern of wall temperature at different flow rates is similar to the Nusselt number, i.e., it transitions from a smooth curve to an oscillation with a certain frequency and gradually increasing amplitude, and the regularity of the oscillation is subsequently disrupted. The location where the regularity is disrupted gradually migrates to the inlet end with the decrease of the flow rate in the tube. The reason for this is the same as the Nusselt number distribution and will not be repeated here. Unlike the Nusselt number curve distribution, the temperature curve amplitude varies greatly at different flow rates, indicating that the residence time of bubbles on the hot wall surface is different at different flow rates. At low flow rates, the bubble attachment time is long and the wall surface locally affected by the bubble experiences a large temperature rise, while at high flow rates, the bubble has difficulty attaching to the wall surface for a long time due to the liquid drag force.

3.4. Comparison of the effects of heat flow density and flow velocity

The distributions of the average wall temperature and the mean Nusselt number under different wall heat flux densities and inlet velocities are shown in Figure 12. Each data point represents the averaged value obtained along the heated wall surface, as calculated by Eqs (10) and (11). Within the range of operating conditions considered in this study, the average wall Nusselt number exhibits a positive correlation with both wall heat flux density and inlet velocity, whereas the average wall temperature shows the opposite trend. These results indicate that both wall heat flux density and inlet velocity can enhance the overall heat transfer performance, with the effect of inlet velocity is more pronounced. Therefore, increasing the inlet velocity is a more effective approach to intensify heat transfer than solely raising the wall heat flux density.

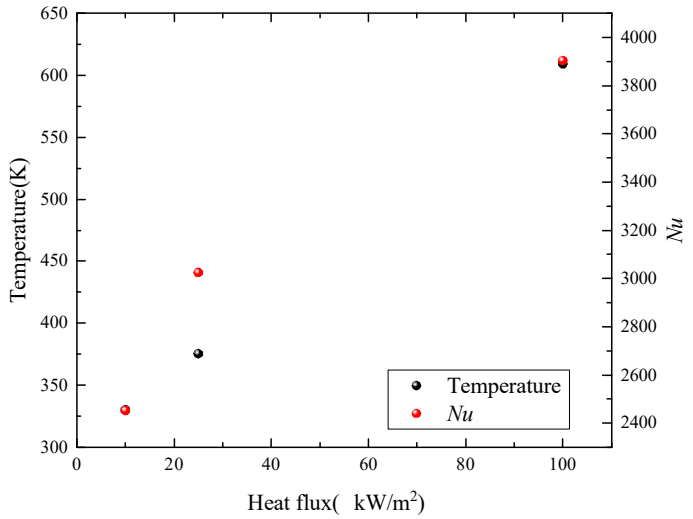

(a) Different heat flow densities

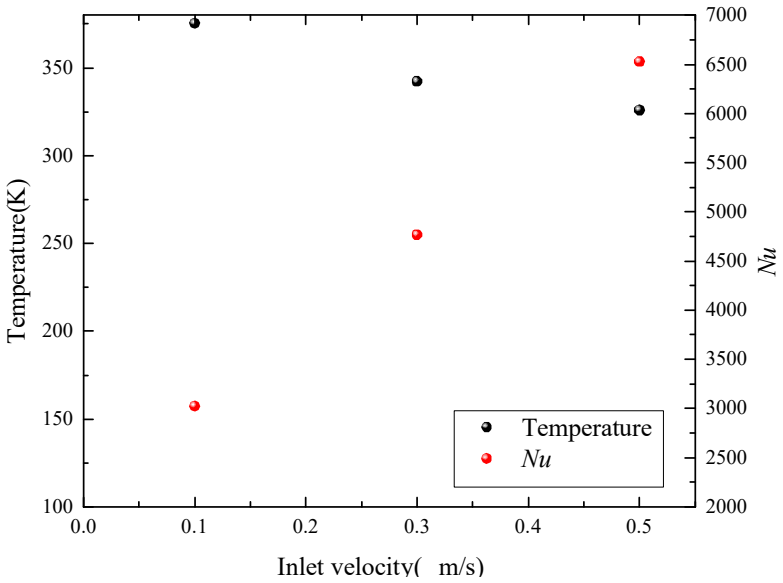

(b) Different flow rates

Figure 12. Mean values of hot wall temperature and Nu number.

The calculation formulas for calculating the average wall temperature under different heat flux densities and flow velocities are as follows:

$$\bar{T} = \sum_{i=1}^{n} T_{w,n} \tag{10}$$

$$\overline{Nu} = \sum_{i=1}^{n} Nu_n \tag{11}$$

Therefore, it is evident that both wall heat flux density and inlet flow velocity can increase the average Nusselt number, with flow velocity having a more significant impact. When the primary goal is to enhance heat transfer, increasing flow velocity is more efficient than merely increasing heat flux density.

4. Conclusions

In this work, the CFD approach based on the volume of fluid (VOF) model was employed to conduct unsteady numerical simulations of the flow-boiling process of the non-azeotropic mixture R601/R601a (1/3) in a horizontal tube. The effects of wall heat flux and inlet velocity on flow-boiling characteristics and heat-transfer performance under the influence of gravity were investigated.

(1) Within the range of operating conditions considered, when the wall heat flux is low, the vapor bubbles are sparsely distributed on the heated surface, the mainstream remains in a subcooled-boiling state, and the wall temperature fluctuates only slightly around its baseline value. When the wall heat flux is high, the bubble distribution becomes denser, the mainstream reaches the saturated-boiling regime, and the wall temperature exhibits stronger and more frequent oscillations.

(2) As the flow velocity increases, the degree of boiling inside the tube gradually decreases. Under low-flow-rate conditions, the low-boiling-point component R601 easily reaches its saturation temperature and dominates the phase-change process. The bubbles generated on the heated wall merge to form a thin vapor film along the upper wall. In contrast, the high-boiling-point component R601a remains in a subcooled-boiling state, where bubbles formed on the wall tend to shrink or collapse within the main flow and cannot rise to the upper wall. The results indicate that, in this non-azeotropic mixture, the low-boiling, more volatile R601 component plays a dominant role in the initial stage of boiling, as its preferential evaporation determines the vapor-phase distribution and governs the flow-pattern transitions at different velocities. Meanwhile, the high-boiling-point R601a component acts as a stabilizing factor, delaying complete vaporization and suppressing excessive temperature fluctuations to maintain system stability.

(3) The average Nusselt number increases with both wall heat flux and flow velocity, while the average wall temperature shows an opposite trend. The enhancement of heat transfer is primarily governed by flow acceleration rather than by thermal loading, because higher flow velocities strengthen convective heat transfer and stabilize the two-phase interface. Therefore, the optimal design of non-azeotropic mixture heat exchangers should consider the balance between component volatility and flow conditions. Increasing the flow velocity is more effective for enhancing heat transfer, while an excessively high heat flux mainly leads to elevated wall temperatures and may induce local dryout. The dominant role of the R601 component in the phase-change process provides a theoretical basis for refrigerant mixture selection and operating condition optimization in heat exchanger design.

Use of AI tools declaration

The authors declare they have not used Artificial Intelligence (AI) tools in the creation of this article.

Acknowledgments

The authors acknowledge the support from the Shihezi University High-Level Talents Research Startup Fund Program (RCZK2025103), the Tianchi Talent Program of Xinjiang Uygur Autonomous Region (2025; Mingfei He), the Shihezi University High-Level Talents Research Startup Fund Program (RCZK2025108), and the Bingtuan Industrial Innovation Research Institute (Bingtuan New Energy Industry Innovation Research Institute, KZ62790101).

Conflict of interest

The authors declare no conflicts of interest.

Author contributions

Chao Huang: Methodology. Xiaohu Liu: Software. Lijiao Gong: Software, Investigation. Mingting Wu: Writing—review & editing, Formal analysis, Data curation. Mingfei He: Visualization, Investigation.

References

1. Li J, Peng X, Yang Z, et al. (2022) Design, improvements and applications of dual-pressure evaporation organic Rankine cycles: A review. *Appl Energy* 311: 118609. https://doi.org/10.1016/j.apenergy.2022.118609
2. Feng YQ, Wang Y, Yao L, et al. (2023) Parametric analysis and thermal-economical optimization of a parallel dual pressure evaporation and two stage regenerative organic Rankine cycle using mixture working fluids. *Energy* 263: 125670. https://doi.org/10.1016/j.energy.2022.125670
3. Xu C, Ma H, Yu X (2024) Comprehensive performance evaluation method of working fluids for high temperature heat pump based on multi-objective optimization. *Appl Therm Eng* 247: 123102. https://doi.org/10.1016/j.applthermaleng.2024.123102
4. Hu Z, Chen Y, Zhang C (2024) Role of R717 blends in ocean thermal energy conversion organic Rankine cycle. *Renewable Energy* 221: 119756. https://doi.org/10.1016/j.renene.2023.119756
5. Liu J, Zhou F, Lyu N, et al. (2023) Analysis of low GWP ternary zeotropic mixtures applied in high-temperature heat pump for waste heat recovery. *Energy Convers Manage* 292: 117381. https://doi.org/10.1016/j.enconman.2023.117381
6. Peng J, Ge Y, Chen F, et al. (2022) Theoretical and experimental study on the performance of a high-efficiency thermodynamic cycle for ocean thermal energy conversion. *Renewable Energy* 185: 734–747. https://doi.org/10.1016/j.renene.2021.12.093
7. Wang Z, Luo L, Xu Z, et al. (2022) Flow boiling of zeotropic mixture R245fa/R141b inside horizontal smooth tube and microfin tube. *Int J Therm Sci* 176: 107504. https://doi.org/10.1016/j.ijthermalsci.2022.107504

8. Xu J, Wang Y, Yang R, et al. (2021) A review of boiling heat transfer characteristics in binary mixtures. *Int J Heat Mass Tran* 164: 120570. https://doi.org/10.1016/j.ijheatmasstransfer.2020.120570
9. Qi Z, Jia L, Dang C, et al. (2024) Heat transfer enhancement for flow boiling of zeotropic mixtures with regulating liquid mass transfer resistance. *Int J Heat Fluid Fl* 107: 109402. https://doi.org/10.1016/j.ijheatfluidflow.2024.109402
10. Banerjee R (2008) Turbulent conjugate heat and mass transfer from the surface of a binary mixture of ethanol/iso-octane in a countercurrent stratified two-phase flow system. *Int J Heat Mass Tran* 51: 5958–5974. https://doi.org/10.1016/j.ijheatmasstransfer.2008.04.057
11. Barroso-Maldonado JM, Montañez-Barrera JA, Belman-Flores JM, et al. (2019) ANN-based correlation for frictional pressure drop of non-azeotropic mixtures during cryogenic forced boiling. *Appl Therm Eng* 149: 492–501. https://doi.org/10.1016/j.applthermaleng.2018.12.082
12. He X, Wang J, Li Z, et al. (2022) Numerical simulation on shell-side flow pattern transition and heat transfer of non-azeotropic refrigerant mixture. *Appl Therm Eng* 214: 118917. https://doi.org/10.1016/j.applthermaleng.2022.118917
13. Zhang W, Cheng M, Zhu X, et al. (2023) Modeling analysis of non-azeotropic and immiscible binary mixed vapors condensation under natural convection. *Int J Heat Mass Tran* 214: 124418. https://doi.org/10.1016/j.ijheatmasstransfer.2023.124418
14. Wang Q, Liu X, Li M, et al. (2023) Numerical simulation of heat transfer characteristics of falling-film evaporation of R32/R134a non-azeotropic refrigerant outside a horizontal tube. *Int Commun Heat Mass* 148: 107001. https://doi.org/10.1016/j.icheatmasstransfer.2023.107001
15. Lv H, Ma H, Zhao Y, et al. (2023) Numerical simulation of flow boiling heat transfer characteristics of R134a/Ethane binary mixture in horizontal micro-tube. *Int J Refrig* 146: 126–134. https://doi.org/10.1016/j.ijrefrig.2022.10.019
16. Xu Y, Han H, Liu L, et al. (2025) Experimental study on the subcooled flow boiling of non-azeotropic mixtures in rhombic fin microchannels. *Int J Heat Mass Tran* 239: 126597. https://doi.org/10.1016/j.ijheatmasstransfer.2024.126597
17. Chen J, Bao L, Xu W, et al. (2024) Experimental study on flow boiling heat transfer characteristics of zeotropic mixture R1233zd (E)/R1234yf in horizontal tube. *Appl Therm Eng* 254: 123942. https://doi.org/10.1016/j.applthermaleng.2024.123942
18. Lu Y, Ling Y, Zhuang Y, et al. (2024) Flow boiling heat transfer characteristics and delayed dry-out ability of non-azeotropic mixtures R245fa/R134a in microchannels. *J Therm Sci* 33: 1174–1188. https://doi.org/10.1007/s11630-024-1959-3
19. Dai B, Wu T, Liu S, et al. (2024) Flow boiling heat transfer characteristics of zeotropic mixture CO2/R152a with large temperature glide in a 2 mm horizontal tube. *Int J Heat Mass Tran* 218: 124779. https://doi.org/10.1016/j.ijheatmasstransfer.2023.124779
20. Huang X, Zhang J, Haglind F (2023) Experimental analysis of high temperature flow boiling of zeotropic mixture R134a/R245fa in a plate heat exchanger. *Appl Therm Eng* 220: 119652. https://doi.org/10.1016/j.applthermaleng.2022.119652
21. Qi Z, Jia L, Dang C, et al. (2022) Liquid mass transfer characteristics of zeotropic mixtures of R134a/R245fa during flow boiling in a rectangular channel. *Int J Heat Mass Tran* 187: 122551. https://doi.org/10.1016/j.ijheatmasstransfer.2022.122551

22. Wang ZQ, Luo L, Xu ZH, et al. (2022) Flow boiling of zeotropic mixture R245fa/R141b inside horizontal smooth tube and microfin tube. *Int J Therm Sci* 176: 107504. https://doi.org/10.1016/j.ijthermalsci.2022.107504
23. ANSYS FLUENT 15.0 in workbench user's guide. (2013) ANSYS Inc., Canonsburg, PA.
24. Hirt CW, Nichols BD (1981) Volume of fluid method for the dynamics of free boundaries. *Computer Phys* 46: 201–225. https://doi.org/10.1016/0021-9991(81)90145-5
25. Brackbill JU, Kothe DB，Zemach C (1992) A continuum method for modeling Surface tension. *Computer Phys* 100: 335–354. https://doi.org/10.1016/0021-9991(92)90240-Y
26. Lee HW (1980) A pressure iteration scheme for two-phase flow modeling. *Washington DC: Hemisphere Publishing* 1: 125–128.
27. LeBlanc C, Ekkad SV, Lambert T, et al. (2013) Detailed heat transfer distributions in engine similar cooling channels for a turbine rotor blade with different rib orientations. *J Turbomachinery* 135: 011034. https://doi.org/10.1115/1.4006387
28. Chiou CB, Lu DC, Liao CY, et al. (2009) Experimental study of forced convective boiling for non-azeotropic refrigerant mixtures R-22/R-124 in horizontal smooth tube. *Appl Therm Eng* 29: 1864–1871. https://doi.org/10.1016/j.applthermaleng.2008.09.004

AIMS Press